Scale effects in gas nano flows

Murat Barisik and Ali Beskok

Citation: Physics of Fluids (1994-present) **26**, 052003 (2014); doi: 10.1063/1.4874678
View online: http://dx.doi.org/10.1063/1.4874678
View Table of Contents: http://scitation.aip.org/content/aip/journal/pof2/26/5?ver=pdfcov
Published by the AIP Publishing

PHYSICS OF FLUIDS **26**, 052003 (2014)

Scale effects in gas nano flows

Murat Barisik and Ali Beskok[a)]
Mechanical Engineering Department, Lyle School of Engineering, Southern Methodist University, Dallas, Texas 75275-0337, USA

(Received 15 November 2013; accepted 21 April 2014; published online 8 May 2014)

Most previous studies on gas transport in nano-scale confinements assume dynamic similarity with rarefied gas flows, and employ kinetic theory based models. This approach is incomplete, since it neglects the van der Waals forces imposed on gas molecules by the surfaces. Using three-dimensional molecular dynamics (MD) simulations of force driven gas flows, we show the significance of wall force field in nano-scale confinements by defining a new dimensionless parameter (B) as the ratio of the wall force-penetration length to the channel height. Investigation of gas transport in different nano-channels at various Knudsen numbers show the importance of wall force field for finite B values, where the dynamic similarity between the rarefied and nano-scale gas flows break down. Comparison of MD results employing molecularly structured three-dimensional walls versus reflection of gas molecules from a two-dimensional planar surface with Maxwell distribution show that the nano-confinement effects cannot be resolved by the latter approach, frequently used in kinetic theory calculations. Molecularly structured walls determine the bulk flow physics by setting a proper tangential momentum accommodation coefficient, and they also determine the transport in the near wall region. Gas nano-flows with finite B exhibit significant differences in the local density and velocity profiles, affecting the mass flow rate and the formation of Knudsen's minimum in nano-channels. © *2014 AIP Publishing LLC*. [http://dx.doi.org/10.1063/1.4874678]

I. INTRODUCTION

Gas flows in nano-channels and pores are observed in several industrial and environmental applications.[1–3] For example, gas separation using nano-membranes can remove carbon dioxide from flue gases to combat global climate change with low capital costs, low energy requirements, and ease in operation.[4–7] When exposed to driving forces such as pressure differences or concentration gradients, nano-engineered composite membranes allow species selective migration of gas molecules through its nano-pores. Another interesting application is in gas recovery from shale reservoirs, where the shale pore sizes are as small as 5 nm.[8–11] Existing theoretical and numerical models are incapable of explaining gas transport in shale reservoirs and nano-pores, which are affected by non-equilibrium and nano-confinement effects.[12–15] While the non-equilibrium effects can be analyzed using the kinetic theory, nano-confinement induces further complications due to the wall-force-field and surface adsorption.

Non-equilibrium gas flows are classified by the Knudsen number ($Kn = \lambda/H$), which is the ratio of the local gas mean free path (λ) to the characteristic length-scale (H), such as the channel height or pore size. Depending on Kn, transport is considered in the continuum ($Kn \leq 0.01$), slip ($0.01 \leq Kn \leq 0.1$), transition ($0.1 \leq Kn \leq 10$), and free-molecular ($Kn > 10$) flow regimes.[16] Within the context of continuum fluid dynamics, constitutive laws used in the definition of stress tensor and heat flux vector and the no-slip boundary condition (BC) break down with increased Knudsen number; first leading to the use of Navier-Stokes equations with slip boundary conditions in the

[a)] Author to whom correspondence should be addressed. Electronic mail: abeskok@lyle.smu.edu. Telephone: (214) 768 3200.

slip flow regime, followed with higher-order continuum descriptions like the Burnett equations in the transition flow regime with high-order slip conditions.[17,18] High Knudsen number flows can be observed when the characteristic dimension decreases or when the fluid becomes more dilute. For the latter case, one utilizes rarefied gas dynamics based on the kinetic theory, which describes low density gas flows in a wide range of *Kn* values.[19–33] Large *Kn* flows are also observed for gas flows in micro- and nano-scale confinements under standard conditions. Most of the earlier studies employed kinetic theory based techniques to explain gas transport in nano-scales. This was justified by matching the Knudsen (*Kn*) and Mach (*Ma*) numbers to maintain the "dynamic similarity" between the low pressure (rarefied) and nano-scale gas flows (note that fixing *Kn* and *Ma*, also fixes the Reynolds number[34]). Unfortunately, this approach neglects the nano-confinement effects, which become increasingly important with the reduced length scales.

Through systematic studies of shear-driven nano-channel flows, we investigated nano-scale confinement effects induced by the wall force field, and have shown that the interactions between gas and wall molecules determine flow physics in the *near wall* and *bulk flow regions*.[35–39] Deficiencies of the current kinetic theory-based approaches in determining the nano-scale gas transport are two folds: First, it is impossible to predict the near wall flow physics; and second, the bulk flow is based on the pre-specified boundary conditions on the surface. Basically, solid surfaces induce forces on fluid molecules resulting in surface induced stresses identified as the "surface virial."[39] For the most simplified case, inter-molecular van der Waals force interactions between the gas and wall molecules extend typically three molecular diameters (∼1 nm) from each wall. This distance is named as the *wall force penetration length*. For a 5 nm channel, 40% of the flow domain experiences the surface force effects, where the transport significantly deviates from the bulk behavior and cannot be predicted by any kinetic theory description. On the other hand, such deviations can be negligible for a 100 nm channel, where only 2% of the flow domain experiences the wall force field. The bulk flow behavior can be predicted using kinetic theory, provided that the specified BC can properly describe the gas/surface interactions. For this purpose, Maxwell-type BCs[40] or other scattering kernels like the Cercignani-Lampis model[41] are frequently employed to describe the reflected molecules at a solid surface. The gas/solid interface is defined as a two-dimensional plane where a Tangential Momentum Accommodation Coefficient (TMAC) is specified to determine tangential momentum exchange between the wall and impinging gas molecules. Unfortunately, TMAC values for specific gas-surface pairs are mostly unknown, creating serious limitations for kinetic theory-based modeling.

One can utilize molecular dynamics (MD) to investigate gas transport in nano-channels. Solid surfaces are molecularly modeled and the surface effects are directly considered by the interactions between gas and surface molecules. In our earlier studies, we characterized the effects of surface force field in nano-scale confined shear driven gas flows by employing the "smart wall" MD (SWMD) algorithm.[35] In addition to the well-known "Knudsen layer" that is about one mean free path long, our results have shown the presence of a near wall sub-layer that is a couple of molecular diameters thick.[35–39] This sub-layer forms due to the gas/surface molecular interactions and cannot be described by kinetic theory. In this layer, the gas density, velocity, shear and normal stress distributions are significantly different than the predictions of the Boltzmann equation.[35–39] Results indicate breakdown of the aforementioned dynamic similarity between rarefied and nano-scale gas flows. Hence, in nano-confined gas flows, *the wall force penetration length* (L_f) emerges as an important length scale in addition to the channel dimensions (H) and gas mean free path (λ).

Objective of this study is to explore the length scales and conditions for applicability of "rarefied gas dynamics" on nano-scale gas flows. We investigate force driven gas flows confined in different height nano-channels, and characterize nano-scale effects on velocity profiles and mass flow rates in the entire Knudsen regime (late slip, transition, and free molecular flow regimes). We also explore the well-known "Knudsen's minimum" for the first time in nano-confinements. Using two different surface definitions, namely, the "molecular BC" and "planar BC" we distinguish the differences between molecular level mechanisms and kinetic theory descriptions, and emphasize the "true" nano-scale effects. By defining the ratio of surface force penetration length (L_f) to the channel height (H) as a new dimensionless parameter ($B = L_f/H$), we will determine the influence of near wall hydrodynamics on the overall gas transport and define validity range of kinetic theory for small scale flows as a function of the B parameter.

This work is organized as follows: In Sec. II, we summarize the *unified transport model* of Beskok and Karniadakis,[42] which provides a theoretical description for pressure driven flows in the entire Knudsen regime. In Sec. III, we describe MD simulation parameters and explain details of the MD algorithm. In Sec. IV, we present gas flow results as a function of modified Knudsen number ($k = \left(\sqrt{\pi}/2\right) Kn$). First, we utilize the "planar BC," which is the fully diffuse reflection of gas molecules from a flat surface with Maxwell distribution, and compare MD results with theoretical predictions. Second, MD boundaries are modeled as molecular surfaces and comparison with theory is established by considering the TMAC value of the studied gas/surface couple. Scale effects are identified by calculating the B parameter, and their influence on transport are characterized by studying mass flow rates in different size nano-conduits. Finally, the conclusions are presented.

II. SUMMARY OF THE UNIFIED FLOW MODEL

Using direct simulation Monte Carlo (DSMC) results and solutions of the linearized Boltzmann (LB) equation in the literature,[17–33] Beskok and Karniadakis[42] developed a phenomenological model that describes the velocity profile, shear stress, pressure gradient, and the mass flow rate in the entire Knudsen regime for rectangular duct and pipe flows. The model is valid for low Mach number compressible gas flows, where the flow is assumed isothermal. The unified model has only two fitting parameters. It captures Maxwell's first-order slip model in the slip flow regime, and reaches the free molecular flow results for $Kn \to \infty$. The model exhibits correct asymptotic behavior both for $Kn \to 0$ and $Kn \to \infty$ limits. An essential component of the model is the *approximation* of the velocity profile with a parabola, which is verified by DSMC and linearized Boltzmann results, as well as the asymptotic analysis of Burnett equations for pressure-driven channel flows.[17,18] Velocity distribution for a pressure driven laminar channel flow of height H is given by

$$U(x, y) = F\left(\frac{dP}{dx}, \mu_0, H, \lambda\right)\left[-\left(\frac{y}{H}\right)^2 + \left(\frac{y}{H}\right) + U_s\right], \tag{1}$$

where $F(dP/dx, \mu_o, H, \lambda)$ shows the functional dependence of velocity magnitude on the pressure gradient, viscosity, channel height, and local mean free path, respectively. Temperature is assumed to be a constant, and therefore, the dynamic viscosity is also a constant. U_s is the velocity slip on the surface which can be modeled by

$$U_s - U_w = \frac{2 - \sigma_v}{\sigma_v}\left[\frac{Kn}{1 - bKn}\left(\frac{\partial U}{\partial n}\right)_s\right], \tag{2}$$

where σ_v is TMAC, b is the general slip coefficient, and U_w is the wall velocity. Using asymptotic analysis of the Navier-Stokes equations, Beskok[42] has shown that value of b depends on the vorticity and vorticity flux on the surface, and Eq. (2) is second-order accurate in Kn in the slip flow regime. For channel and pipe flows $b = -1$. In addition, setting $b = 0$ recovers the Maxwell's first-order slip boundary condition. Essentially, Eq. (2) is a Padé approximation or regularization that would result in finite slip even when $Kn \to \infty$. Using Eq. (2), and $b = -1$, Eq. (1) becomes

$$U(x, y) = F\left(\frac{dP}{dx}, \mu_0, H, \lambda\right)\left[-\left(\frac{y}{H}\right)^2 + \left(\frac{y}{H}\right) + \left(\frac{2 - \sigma_v}{\sigma_v}\right)\frac{Kn}{1 + Kn}\right]. \tag{3}$$

Assuming this form of the velocity distribution, channel average velocity becomes

$$\bar{U}(x) = F\left(\frac{dP}{dx}, \mu_0, H, \lambda\right)\left[\frac{1}{6} + \left(\frac{2 - \sigma_v}{\sigma_v}\right)\frac{Kn}{1 + Kn}\right]. \tag{4}$$

By non-dimensionalizing the velocity distribution with the local average velocity, dependence on the local flow conditions given by $F(dP/dx, \mu_o, H, \lambda)$ is eliminated. Therefore, the normalized velocity profile of a Poiseuille flow can be obtained as a function of Kn, y, and σ_v as

$$U^*(y, Kn) \equiv \frac{U(x, y)}{\bar{U}(x)} = \left[\frac{-\left(\frac{y}{H}\right)^2 + \left(\frac{y}{H}\right) + \left(\frac{2 - \sigma_v}{\sigma_v}\right)\frac{Kn}{1 + Kn}}{\frac{1}{6} + \left(\frac{2 - \sigma_v}{\sigma_v}\right)\frac{Kn}{1 + Kn}}\right]. \tag{5}$$

Once the shape of the normalized velocity profile is fixed, the *unified transport model* of Beskok and Karniadakis (BKM) models the mass flow rate by exploiting the functional dependence of $F(dP/dx, \mu_o, H, \lambda)$ using Navier-Stokes equations, but the model also recognizes the role of viscous diffusion via a Knudsen number dependent diffusion coefficient that would converge to the dynamic viscosity in the slip and continuum flow regimes ($\mu_0 = (\rho\lambda c)/3$, where c is the local speed of sound). However, for collisionless flows (i.e., $Kn \rightarrow \infty$) the diffusion coefficient is determined by the channel size H rather than the local mean free path λ. This process requires introduction of a rarefaction coefficient that is zero in the continuum and slip-flow regimes, and becomes a known constant of order unity in the free molecular flow regime. In fact, the switch between zero and a known constant in the model happens around $Kn = 1$. This enables a global curve-fitting (for $0 \leq Kn < \infty$) of the existing mass flow rate data using only two parameters. Further details of this model can be found in Ref. 42.

III. THREE-DIMENSIONAL MD SIMULATION DETAILS

Pressure-driven gas flows can be simulated by forming a density gradient along the stream-wise direction. However, this requires modeling of very long nano-channels with inlet and outlet reservoirs at different gas densities and pressures. Such approach is not feasible using MD. To circumvent this difficulty, we *simulated force-driven flows, which are hydrodynamically identical to low Mach number pressure-driven gas flows*. Force-driven flows greatly simplify MD simulations by imposing periodicity in the stream-wise direction that is typically λ long. Hence, density gradient in the stream wise direction is neglected for such small distances (i.e., λ).

We simulated force driven argon gas flows between two parallel plates separated with a distance H using our three-dimensional MD algorithm. Periodic boundary conditions are applied in the stream wise and lateral directions. Size of the domain is crucial especially in the flow direction to simulate correct gas thermodynamic state.[35] In order to capture gas/gas intermolecular collisions, simulation domains span 54 nm ($\sim \lambda_{Ar}$) in the periodic directions. A constant driving force (F_{drive}) is applied on each gas molecule in the stream wise direction, while the applied force is specified according to the flow area and the boundary definition employed. Specifically, F_{drive} is adjusted to create $Ma \approx 0.2$ gas velocity at the channel center in order to maintain isothermal and nearly incompressible flow conditions in all cases. For example, for the molecular BC cases, F_{drive} is fixed at 1.224×10^{-13} N/atom in the 5.4 nm height channels (5.4 nm $\times$ 54 nm flow area) while the 54 nm channel cases (54 nm $\times$ 54 nm flow area) use $F_{drive} = 1.224 \times 10^{-14}$ N/atom.

Thermodynamic state of argon at 298 K and 113.4 kPa corresponds to a density of $\rho_{Ar} = 1.896$ kg/m^3, and $\lambda_{Ar} = 54$ nm. By keeping the gas temperature at 298 K, pressure is varied in order to obtain different λ values. Mean molecular spacing values of each case are checked, and the thermodynamic states are validated to be dilute gas, obeying the ideal gas law. Local gas temperature is also computed throughout the channels to ensure isothermal conditions.

This study employs two different surface definitions; a kinetic theory based planar boundary condition and atomistically modeled surfaces. In the first approach, diffuse reflection of gas molecules from an isothermal flat surface with Maxwell distribution frequently utilized in kinetic theory is used. With fully diffuse gas/surface interaction assumption, all three components of the velocity are reset according to a "biased Maxwellian distribution" when a gas particle strikes the surface.[43] Distribution function for gas velocity normal to the surface, $f(v_y)$, is assigned as

$$f(v_y) = \frac{m_{Ar} v_y}{k_b T_w} e^{-\frac{m v_y^2}{2 k_b T_w}}, \tag{6}$$

where v_y is the gas velocity normal to the surface, k_b is the Boltzmann constant (1.3806×10^{-23} J K^{-1}), and T_w is the wall temperature (298 K). Distribution function for gas velocities parallel to the surface are defined as

$$f(v_x) = \sqrt{\frac{m_{Ar}}{2\pi k_b T_w}} e^{-\frac{m v_x^2}{2 k_b T_w}} \text{ and } f(v_z) = \sqrt{\frac{m_{Ar}}{2\pi k_b T_w}} e^{-\frac{m v_z^2}{2 k_b T_w}}. \tag{7}$$

In order to validate the use of Eqs. (6) and (7) in the MD code, the x- and y-direction velocity distributions of reflected molecules are measured in MD, and compared with the corresponding

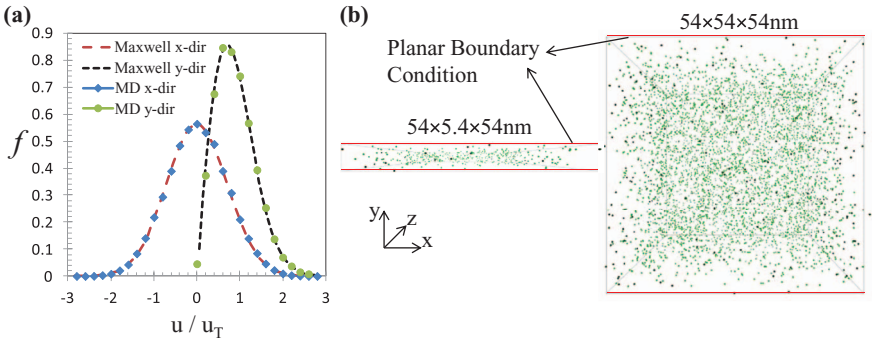

FIG. 1. (a) Velocity distribution function, f, of molecules parallel (in x-direction) and normal (in y-direction) to the surface. Shapes show MD results while the dashed lines show Maxwell distributions given by Eqs. (6) and (7). (b) MD simulation snapshots of 5.4 nm and 54 nm height channels using planar boundary conditions.

Maxwell distributions in Figure 1(a). Snapshots of MD simulation domains with planar BC for two different channel heights of 5.4 nm and 54 nm are given in Figure 1(b).

In order to demonstrate the importance of molecular modeling of surfaces, the second set of MD simulations utilized three-dimensional FCC crystal structured walls with 0.54 nm cubic unit cell length and (100) plane facing the gas molecules. Since gas molecules interact through intermolecular collisions, MD simulation domains must be at least one mean free path long in the periodic directions.[35] This greatly complicates MD simulations, where the number of wall molecules overwhelms the simulation. We addressed this computational difficulty by introducing and using the Smart Wall Molecular Dynamics (SWMD) algorithm, which reduces the memory requirements for modeling surfaces. For three-dimensional FCC crystal structured walls used here, the SWMD limits memory use of a semi-infinite wall slab into a stencil of 74 wall molecules.[35] The current SWMD is a fixed lattice model, where the wall molecules are rigid and keep their corresponding FCC positions (i.e., cold wall model). When a gas molecule approaches the surface and enters the near wall region, the SWMD wall stencil models semi-infinite wall. Figure 2(a) schematically shows this procedure, where patchy walls appearing on MD boundaries in Figure 2(b) show SWMD stencils during a simulation. Although there are many wall stencils at a given instant, all of these are modeled using the same 74 wall molecules shown on the top of Figure 2(a), resulting in significant computational advantages.[35]

Lennard-Jones (L-J) 6-12 potential is utilized to model the van der Waals interactions between gas-gas and gas-wall molecules. The truncated (6-12) L-J potential is given as

$$V_{truncated}(r_{ij}) = 4\varepsilon\left(\left(\left(\frac{\sigma}{r_{ij}}\right)^{12} - \left(\frac{\sigma}{r_{ij}}\right)^{6}\right) - \left(\left(\frac{\sigma}{r_c}\right)^{12} - \left(\frac{\sigma}{r_c}\right)^{6}\right)\right), \tag{8}$$

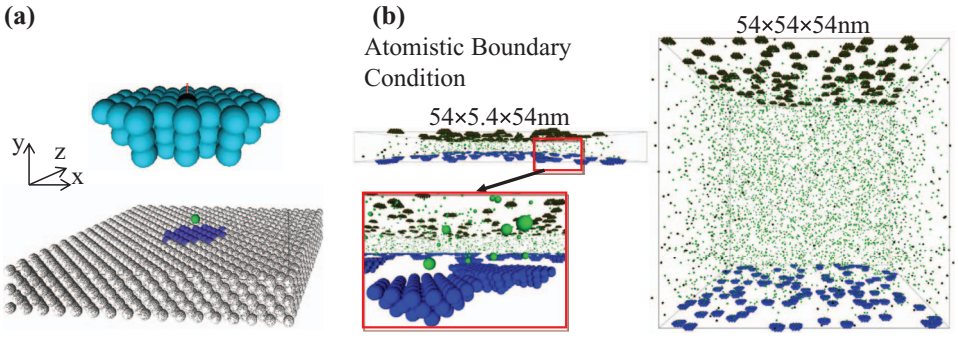

FIG. 2. (a) Illustration of the SWMD procedure. (b) MD simulation snapshots of 5.4 nm and 54 nm height channels with atomistic BC.

where r_{ij} is the intermolecular distance, ε is the depth of the potential well, σ is the molecular diameter, and r_c is the cut-off radius. In this study, we utilize $r_c = 1.08$ nm, which is approximately equal to 3.17σ for argon molecules. At this cut-off-distance, the attractive part of the L-J potential is reduced to 0.00392ε. Our algorithm utilizes the well-known link cell method to handle particle-particle interactions.[44] Mass for an argon molecule is $m_{Ar} = 6.63 \times 10^{-26}$ kg, its molecular diameter is $\sigma_{Ar} = 0.3405$ nm, and the depth of the potential well for argon is $\varepsilon_{Ar} = 119.8 \times k_b$. The latter parameter defines the gas-gas interaction strength, and it is identified as ε_{ff}. For simplicity, the walls have molecular mass and diameter equivalent to argon ($m_{\text{wall}} = m_{\text{Ar}}$, $\sigma_{\text{wall}} = \sigma_{\text{Ar}}$). Since the wall molecules are fixed in the cold wall model, the wall's molecular mass has no effect in the momentum exchange between the gas and wall molecules. In addition, the molecular diameter between different species does not vary drastically. In this study, we also utilized the potential strength for gas–wall interactions to be the same with that of gas–gas molecular interactions ($\varepsilon_{wf} = \varepsilon_{ff}$).

Simulations start from the Maxwell-Boltzmann velocity distribution for gas molecules at 298 K. Initial particle distribution is evolved 10^6 time-steps (4 ns) to reach an isothermal steady state using 4 fs ($\sim 0.002\tau$) time steps, after which, 2×10^6 time steps (8 ns) are performed for time averaging. Longer time averaging has also been performed to confirm the convergence of density, stress, and velocity profiles to steady state. In order to capture the property variations within the near wall region accurately and with same resolution, all simulation domains are divided into 100 slab bins in the wall normal direction. Canonical ensemble (*NVT*, i.e., constant mole, N, volume, V, and temperature, T) is performed by utilizing a thermostat. We employed the Nose-Hoover algorithm[45] as a global thermostat inside the local sub-domains to obtain isothermal conditions at 298 K with a relaxation time of ~0.2 ps. Sub-domains have 0.54 nm heights through the entire span which is 10 times larger than the utilized bin size.

IV. RESULTS AND DISCUSSION

A. Nano-scale gas flows with planar BC

We start our study by applying diffuse reflection of gas molecules from an isothermal flat surface with Maxwell distribution, identified as the "planar BC." Ignoring the nanoscopic corrugations of the surface molecular structure and the force field induced by the surface on gas molecules, the gas/surface interactions are defined by Eqs. (6) and (7) with a fully diffuse assumption, where TMAC = 1. We simulate 5.4 nm and 54 nm height channels, while different k flows are established by varying the gas pressure. For example, in a 5.4 nm channel, argon gas at standard conditions results in $k = 10$ (i.e., free molecular flow regime), while increasing the gas pressure ten times creates the $k = 1$ case, which is in the transition flow regime.

Gas density distributions normal to the surface are found constant without any variations in the near surface region for all cases. This shows that surface adsorption of gas molecules and its effects on transport cannot be considered by using such interface definition. MD velocity profiles of fully developed force driven $k = 10$ flows obtained in 5.4 nm and 54 nm height channels, and $k = 1$ flows in 5.4 nm and 54 nm channels are shown in Figure 3. Velocity profiles normalized with the mean gas velocity (u_M) are plotted in the half of the channel through the non-dimensional height. The LB[46] and BKM[42] solutions of $k = 10$ and $k = 1$ flows at TMAC = 1 are also given. As shown in Figure 3(a), MD $k = 10$ flows in 5.4 nm and 54 nm height channels are identical with LB and BKM solutions. Likewise, $k = 1$ flows of different height channels given in Figure 3(b) are similar with the kinetic theory predictions, regardless of the channel height. This validates that, if the Maxwell-type planar BC is employed, any molecular simulation of a specified *Kn* flow *in any scale* converges to the same velocity profile. Indeed, this is the main idea of *dynamic similarity* at a fixed *Kn* value. Hence, the kinetic theory cannot distinguish any difference between $k = 10$ flow in 5.4 nm and 54 nm channels, and cannot properly consider the size effects. We also have two additional outcomes here: First, LB provides very accurate description for small scale flows if *the scale effects are negligible*; second, MD modeling using a Maxwell-type planar BC is unnecessary, since the same results can be obtained using DSMC with considerably lower computational costs.

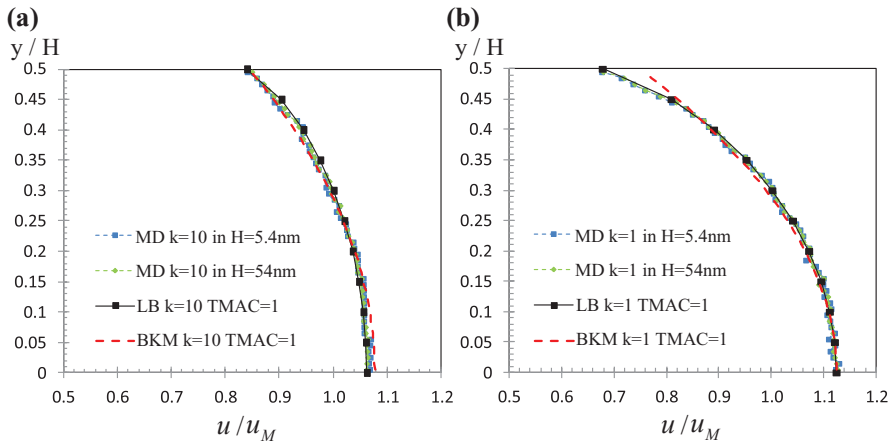

FIG. 3. Velocity profiles of (a) $k = 10$ and (b) $k = 1$ MD gas flows using planar BC. Linearized Boltzmann (LB) solutions[46] and Beskok and Karniadakis model (BKM)[42] (Eq. (5)) predictions of $k = 10$ and $k = 1$ flows for the fully diffuse case (TMAC = 1) are given for comparison.

B. Nano-scale gas flows with molecular BC

In these sets of simulations, MD boundaries are modeled as molecular surfaces using the SWMD algorithm. Details of the FCC structured solid surface and gas/solid interaction parameters are given in Sec. III. We start with 54 nm height channel, where $k = 10$, 1, and 0.1 flows are created by varying the gas pressure. Different than the previous case, gas molecules adsorbed on atomistic surfaces increases gas density near the surface within the *wall force penetration depth*, after which uniform density is observed in the bulk of the channel. This region is too thin to be shown for the 54 nm thick channel and the density profiles will be shown for the 5.4 nm channel cases. Figure 4 shows the velocity profiles in 54 nm height channels, which are parabolic in the bulk of the channel. In the near wall region, sudden decrease of gas velocity is observed. Due to the surface forces which are effective through "the wall force penetration length," velocity profiles diverge from the kinetic theory predictions inside this near surface sublayer. For the current cases, a proper comparison of MD results with LB and BKM is obtained by normalizing the velocity profiles without the influence of the near surface transport. Hence, we employed a mean velocity (u_M^*) defined in the bulk by excluding the near surface regions shown with gray dashed-dotted line in Figure 4. In our earlier works,[37–39] same surface definition is studied for shear driven flow cases where TMAC value of this surface/gas couple was calculated to be 0.75, which was shown to be independent of the channel

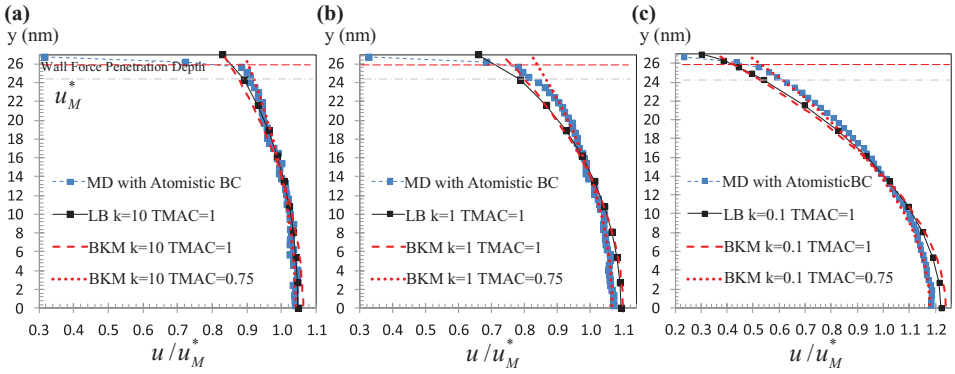

FIG. 4. Velocity profiles for (a) $k = 10$, (b) $k = 1$, and (c) k = 0.1 gas flows confined in 54 nm height channels obtained by MD and employing atomistic walls. Linearized Boltzmann[46] solution for TMAC = 1, and Beskok and Karniadakis model[42] (Eq. (5)) for TMAC = 1 and TMAC = 0.75 are given for comparisons.

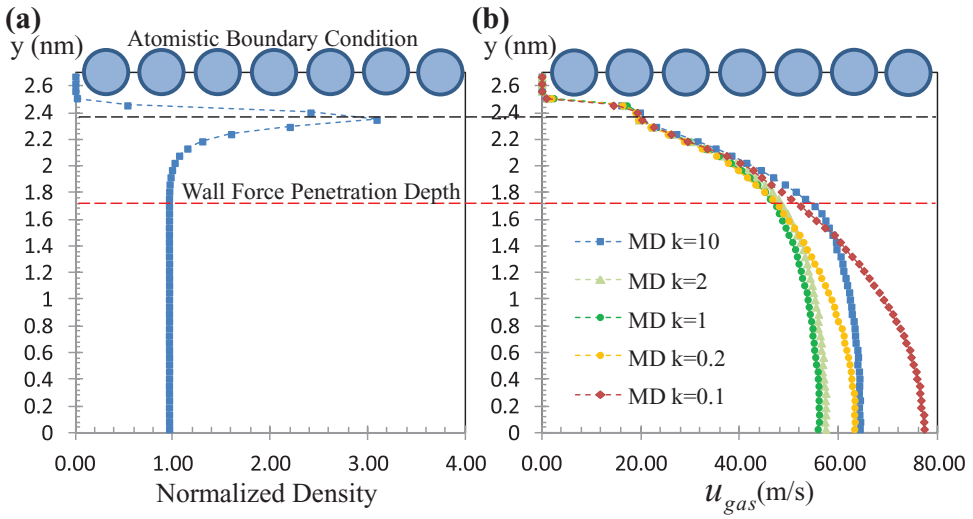

FIG. 5. (a) Gas density distribution in the half of the 5.4 nm height channel obtained using molecular representation of the walls. Figure also includes a schematic of the atomistic BC with wall molecules to emphasize the scales involved in the problem. (b) Velocity profiles for $k = 10$, 2, 1, 0.2, and 0.1 gas flows confined in 5.4 nm height channels with atomistic BC.

height, gas density, and Knudsen number. Based on this knowledge, solutions of BKM for $k = 10$, 1, and 0.1 flows with TMAC = 0.75 are given, in addition to the LB and BKM results with TMAC = 1. The MD velocity profiles agree well with the kinetic theory predictions of TMAC = 0.75 flows in the bulk region, and the differences between the TMAC = 0.75 and 1 flows become more distinguishable for low k values, which is due to normalization by the mean velocity.

The results in Figure 4 indicate that kinetic theory can predict the velocity distribution in the bulk if the TMAC value is known. Considering a small confinement case, where the surface forces are effective in *very limited portion of the flow domain*, BKM solution will be sufficient to model the transport. At this point, we define the new dimensionless parameter, B, to describe the influence of surface forces on the overall flow field. B is the ratio of force penetration length (L_f) to the channel height (H) as $B = L_f / H$, which is 0.02 for the studied 54 nm channel with van der Waals surface forces. Thus, surface forces are effective in approximately 4% ($2 \times B\%$) of the 54 nm height channel, which can be considered as negligible.

For the 5.4 nm height channel cases, the near wall region and wall force field become dominant, where $B = 0.2$. In order to emphasize the scales involved in this case, a schematic of the atomistic BC with the wall molecules is presented in Figure 5. First of all, the density profile in half of the 5.4 nm channel is shown in Figure 5(a) to discuss the molecular level mechanisms inside the wall force penetration length. Gas density near the surface increases almost three times with a single peak point at one molecular diameter (σ) away from surface, representing accumulation near the surface. This behavior is due to the surface potentials increasing the residence time of particles inside the force penetration depth. Molecules are not *immobilized* on the surface. Instead, they are trapped in the wall potential field for a certain time period, and experience multiple collisions with the surface. Since the simulation domains are in equilibrium, some of the trapped particles can leave and resume their free flights, while new particles get inside the force penetration region. Therefore, the density distribution both in the bulk and near wall regions remains unchanged at any flow condition. The density particularly starts to deviate from its bulk value around 2.5σ from the surface. The wall is defined at the center of the first row of wall molecules facing the fluid. As a result, gas molecules cannot penetrate to several bins neighboring the wall, and the gas density goes to zero within 0.2 nm from the wall. In such small scales, difficulty in defining the exact location of the gas/solid interface adds additional constrains for a possible kinetic theory description.

Velocity profiles of $k = 10$, 2, 1, 0.2, and 0.1 MD gas flows confined in 5.4 nm height channel are given in Figure 5(b). A constant driving force of 1.224×10^{-13} N/atom creates different velocity

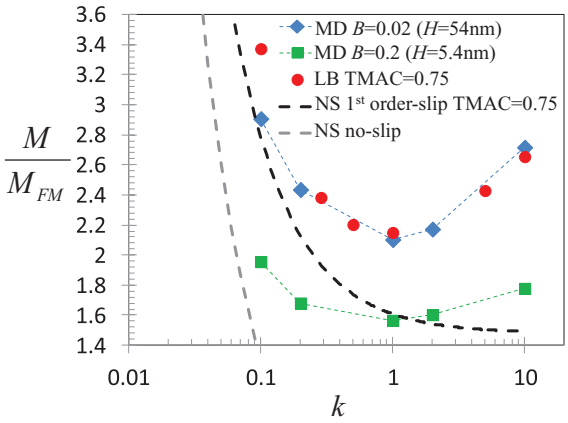

FIG. 6. Free-molecular scaling of MD mass flow rates for 54 nm and 5.4 nm height channels using atomistic BC. LB results for TMAC = 0.75 are adopted from Ref. 47. Mass flow rate results of Navier-Stokes solution using no-slip and first order-slip boundary conditions on the surface are also shown.

profiles at different k flows depending on the rarefaction level. With a simple consideration, the lowest gas velocity at the channel center is observed for $k = 1$ flow case, while the center velocity increases with both increase and decrease of k from unity. The velocity distribution at any k value cannot be described by a parabolic profile. Basically, gas velocities for different k flows behave as follows: (1) They reach zero in the zero density bins near the gas/solid interface, (2) they increase with a sudden jump to a constant value regardless of k at one molecular diameter (σ) away from the surface, and (3) they show a similar increasing trend up to the edge of the wall force penetration depth, after which, the velocity distribution differs based on the k value. Hence, the results show that gas flows in a 5.4 nm channel cannot be predicted by a kinetic theory based procedure both in the bulk and near wall regions at any k value through the entire Knudsen regime.

In addition to the velocity profiles, gas mass flow rates are studied as a function of k and B parameters, in order to establish a complete understanding of the size effects on nano-scale gas transport. The normalized mass flow rates measured in 5.4 nm ($B \approx 0.2$) and 54 nm ($B \approx 0.02$) channels are plotted in Figure 6 as a function of k. Based on the kinetic theory of gases, mass flow rate per unit width for a force driven flow between two parallel plates in the free molecular regime ($k \to \infty$) can be estimated as

$$M_{FM} = \frac{H^2}{\sqrt{2R_{Ar}T_{Ar}}}\rho_{Ar}\frac{F_{drive}}{m_{Ar}}, \tag{9}$$

where R is the specific gas constant ($R_{Ar} = 208$ J/kg K). This equation gives an order of magnitude for the mass flow rate in the free molecular flow regime, which shows variations based on the channel aspect ratio.[17] MD results are normalized using Eq. (9) and the corresponding channel height, gas density, and driving force for each case. The LB solution of mass flow rates at various k values are provided from Sharipov for TMAC = 0.75.[47] For low B flow in 54 nm channel, MD results show great agreement with LB in a wide k range. However, there is a mismatch between the MD and LB results for $k = 0.1$. In order to explain this, we utilized Maxwell's first order slip correction (obtained by using Eq. (2) with $b = 0$), and analytical solution of the Navier-Stokes equation for force driven gas flows, which results in mass flow rate per unit width

$$M_{Slip} = \rho_{Ar}^2\frac{F_{drive}}{m_{Ar}}\frac{H^3}{2\mu}\left(\frac{1}{6} + \frac{(2-\sigma)}{\sigma}Kn\right). \tag{10}$$

One must note that $\rho_{Ar}F_{drive}/m_{Ar}$ used in Eqs. (9) and (10) replaces the local pressure gradient terms in the free molecular flow solution of the Boltzmann equation,[17] and in the Navier-Stokes equation.

Normalization of Eq. (10) with the free molecular mass flow rate in Eq. (9) gives

$$\frac{M_{Slip}}{M_{FM}} = \frac{\pi}{4k}\left(\frac{1}{6} + \frac{(2-\sigma)}{\sigma}\frac{2}{\sqrt{\pi}}k\right), \tag{11}$$

where $\lambda = (\mu/\rho)\sqrt{\pi/2RT}$ is used. First term on the right hand side is inversely proportional to k, and represents the normalized mass flow rate for Navier-Stokes equation with no-slip boundary condition, while the term proportional to k is due to Maxwell's first-order slip boundary condition. Gas mass flow rate predictions for both no-slip and first order-slip boundary conditions on the surface are also plotted in Figure 6. Equation (11) is expected to give an accurate description of flow rate for $k \leq 0.1$. MD and first-order slip results show great agreement at $k = 0.1$, while LB over-estimates the mass flow rate. This validates that MD can successfully model gas flows from slip to free molecular flow regimes.

Variation of mass flow rate as a function of k in Figure 6, show the "Knudsen's Minimum,"[48,49] investigated both experimentally[50] and theoretically.[46,51–53] Interestingly, MD can capture this behavior in nano-scale flows. Knudsen's minimum is observed around $k = 1$. Basically, the mass flow rate decreases with an increase of k due to the rarefaction (non-continuum) effects up to $k = 1$. Further increase in k results in increased flow rate. However, different than the kinetic theory description, MD results show further dependence on B parameter in addition to k. While the variation of transport observed in LB solution solely depends on the rarefaction level, MD reveals size effects as a function of B. For the 54 nm channel cases, mass transport still varies *mostly* based on the rarefaction effects defined by k since the surface force effects represented by B parameter is negligible ($B = 0.02$). However, in 5.4 nm channel B reaches a finite value ($B = 0.2$), and the mass flow rates become a function of both rarefaction and nano-scale effects. Basically, the surface forces dominate over rarefaction by reducing the mass flow rate, and suppressing its variation by *Knudsen* number.

V. CONCLUSION

Surface force field can dominate the flow physics in nano-scale depending on the characteristic dimension of the confinement. Existing kinetic theory based approaches do not consider such mechanism, and provide solution for nano-scale gas flows regardless of the scale effects. In order to identify the scale effects, we defined a dimensionless parameter B as the ratio of the wall force penetration length to the local channel height, where finite values of B show significance of the wall force-field. Using three-dimensional MD simulations of force driven gas flows with planar boundary conditions and molecularly structured walls, we investigated gas flows varying from the slip to free molecular flow regimes in two different nano-channels. Our findings show the following: First, molecularly structured walls determine bulk transport by setting the TMAC value regardless of the confinement effects determined by the B parameter. Therefore, kinetic theory based models can properly predict gas transport when $B \to 0$, provided that a proper TMAC value is specified. The near-wall physics has very limited effect on the mass transport for such cases. Second, the molecularly structured walls also determine transport in the near wall region, which shows significant deviations from the kinetic theory predictions. This region becomes dominant for finite values of B, and the near wall region interacts with the bulk flow, resulting in completely different velocity profiles and mass transport in nano-channels. Hence, the well-known Knudsen's minimum in mass transport manifests itself differently for gas nano-flows with finite B values. We have shown that the dimensional limit of kinetic theory based descriptions of gas nano-flows are defined by the B parameter, where dynamic similarity between rarefied and nano-flows are valid only for $B \to 0$, while finite values of B require modeling of the wall force field effects. MD simulations of gas flows enable proper investigations of the non-equilibrium and confinement effects, revealing the influence of wall-force-field and surface adsorption on transport.

Potential strength of the gas–wall interactions determines the near-wall physics, including the surface adsorption. Our future work will include systematic studies by variation of the gas-wall interaction potential, along with the variations in the scale (B) and rarefaction (k) parameters, which will enable further exploration of gas transport through nano-membranes and nano-pores.

[1] M. Majumder, N. Chopra, and B. J. Hinds, "Mass transport through carbon nanotube membranes in three different regimes: Ionic diffusion and gas and liquid flow," ACS Nano **5**(5), 3867–3877 (2011).
[2] N. Halonen, A. Rautio, A. R. Leino, T. Kyllonen, G. Toth, J. Lappalainen, and R. Vajtai, "Three-dimensional carbon nanotube scaffolds as particulate filters and catalyst support membranes," ACS Nano **4**(4), 2003–2008 (2010).
[3] D. Yoon, C. Lee, J. Yun, W. Jeon, B. J. Cha, and S. Baik, "Enhanced condensation, agglomeration, and rejection of water vapor by superhydrophobic aligned multiwalled carbon nanotube membranes," ACS Nano **6**(7), 5980–5987 (2012).
[4] B. Li, B. Jiang, D. J. Fauth, M. L. Gray, H. W. Pennline, and G. A. Richards, "Innovative nano-layered solid sorbents for CO_2 capture," Chem. Commun. **47**(6), 1719–1721 (2011).
[5] S. R. Venna and M. A. Carreon, "Highly permeable zeolite imidazolate framework-8 membranes for CO_2/CH_4 separation," J. Am. Chem. Soc. **132**(1), 76–78 (2010).
[6] W. Yave, A. Car, J. Wind, and K. V. Peinemann, "Nanometric thin film membranes manufactured on square meter scale: Ultra-thin films for CO_2 capture," Nanotechnology **21**(39), 395301 (2010).
[7] M. T. Ho, G. W. Allinson, and D. E. Wiley, "Reducing the cost of CO_2 capture from flue gases using membrane technology," Ind. Eng. Chem. Res. **47**(5), 1562–1568 (2008).
[8] R. G. Loucks, R. M. Reed, S. C. Ruppel, and D. M. Jarvie, "Morphology, genesis, and distribution of nanometer-scale pores in siliceous mudstones of the Mississippian Barnett Shale," J. Sedimen. Res. **79**(12), 848–861 (2009).
[9] G. King, "Thirty years of gas shale fracturing: What have we learned?," in *Proceedings of the SPE Annual Technical Conference and Exhibition, Florence, Italy*, 19–22 September 2010.
[10] S. L. Montgomery, D. M. Jarvie, K. A. Bowker, and R. M. Pollastro, "Mississippian Barnett Shale, Fort Worth basin, north-central Texas: Gas-shale play with multi-trillion cubic foot potential," AAPG Bull. **89**(2), 155–175 (2005).
[11] K. K. Chong, W. Grieser, A. Passman, H. Tamayo, N. Modeland, and B. Burke, "A completions guide book to shale-play development: A review of successful approaches toward shale-play stimulation in the last two decades," in *Proceedings of the Canadian Unconventional Resources and International Petroleum Conference, Calgary, AB, Canada*, 19–21 October 2010.
[12] G. Michel, R. Sigal, F. Civan, and D. Devegowda, "Parametric investigation of shale gas production considering nano-scale pore size distribution, formation factor, and non-Darcy flow mechanisms," in *Proceedings of the SPE Annual Technical Conference and Exhibition, Denver, CO, USA*, 30 October–2 November 2011.
[13] F. Civan, "Effective correlation of apparent gas permeability in tight porous media," Transp. Porous Media **82**(2), 375–384 (2010).
[14] F. Civan, "A review of approaches for describing gas transfer through extremely tight porous media," AIP Conf. Proc. **1254**, 53 (2010).
[15] F. Civan, C. S. Rai, and C. H. Sondergeld, "Shale-gas permeability and diffusivity inferred by improved formulation of relevant retention and transport mechanisms," Transp. Porous Media **86**(3), 925–944 (2011).
[16] S. A. Schaaf and P. L. Chambre, *Flow of Rarefied Gases* (Princeton University Press, Princeton, NJ, 1966).
[17] G. E. Karniadakis, A. Beskok, and N. Aluru, *Micro Flows and Nano Flows: Fundamentals and Simulation* (Springer-Verlag, New York, 2005).
[18] A. Beskok, "Simulations and models for gas flows in microgeometries," Ph.D. thesis (Princeton University, Princeton, NJ, 1996).
[19] Y. Sone, S. Takata, and T. Ohwada, "Numerical analysis of the plane Couette flow of a rarefied gas on the basis of the linearized Boltzmann equation for hard sphere molecules," Eur. J. Mech. B/Fluids **9**, 273–288 (1990).
[20] S. Fukui and R. Kaneko, "A database for interpolation of Poiseuille flow rates for high Knudsen number lubrication problems," J. Tribol. **112**, 78–83 (1990).
[21] S. Fukui and R. Kaneko, "Analysis of ultra-thin gas film lubrication based on the linearized Boltzmann equation: Influence of accommodation coefficient," JSME Int. J. **30**, 1660–1666 (1987).
[22] D. Singh, X. Guo, A. Alexeenko, J. Y. Murthy, and T. S. Fisher, "Modeling of subcontinuum thermal transport across semiconductor-gas interfaces," J. Appl. Phys. **106**, 024314 (2009).
[23] M. A. Gallis, J. R. Torczynski, D. J. Rader, M. Tij, and A. Santos, "Normal solutions of the Boltzmann equation for highly nonequilibrium Fourier flow and Couette flow," Phys. Fluids **18**, 017104 (2006).
[24] D. Valougeorgis and S. Naris, "Analytical lattice Boltzmann solutions for thermal flow problems," Transp. Theory Stat. Phys. **32**, 645–656 (2003).
[25] S. Narisa, D. Valougeorgisa, D. Kalempab, and F. Sharipov, "Gaseous mixture flow between two parallel plates in the whole range of the gas rarefaction," Physica A **336**, 294–318 (2004).
[26] G. A. Bird, *Molecular Gas Dynamics and the Direct Simulation of Gas Flows* (Oxford Science Publications, Midsomer Norton, Avon, UK, 1994).
[27] J. H. Park, P. Bahukudumbi, and A. Beskok, "Rarefaction effects on shear driven oscillatory gas flows: A DSMC study in the entire Knudsen regime," Phys Fluids **16**(2), 317–330 (2004).
[28] P. Bahukudumbi, J. H. Park, and A. Beskok, "A unified engineering model for steady and quasi-steady shear-driven gas microflows," Microscale Thermophys. Eng. **7**, 291–315 (2003).
[29] X. Guo and A. Alexeenko, "Compact model of squeeze-film damping based on rarefied flow simulations," J. Micromech. Microeng. **19**, 045026 (2009).
[30] M. A. Gallis and J. R. Torczynski, "An improved Reynolds-equation model for gas damping of microbeam motion," J. Microelectromech. Syst. **13**(4), 653–659 (2004).
[31] W. D. Zhou, B. Liu, S. K. Yu, and W. Hua, "Rarefied-gas heat transfer in micro- and nanoscale Couette flows," Phys. Rev. E **81**, 011204 (2010).
[32] D. J. Rader, M. A. Gallis, J. R. Torczynski, and W. Wagner, "Direct simulation Monte Carlo convergence behavior of the hard-sphere-gas thermal conductivity for Fourier heat flow," Phys. Fluids **18**, 077102 (2006).
[33] G. A. Bird, M. A. Gallis, J. R. Torczynski, and D. J. Rader, "Accuracy and efficiency of the sophisticated direct simulation Monte Carlo algorithm for simulating noncontinuum gas flows," Phys. Fluids **21**, 017103 (2009).

[34] A. Beskok and G. E. Karniadakis, "Simulation of heat and momentum transfer in complex micro-geometries," J. Thermophys. Heat Transfer **8**(4), 647–655 (1994).
[35] M. Barisik, B. Kim, and A. Beskok, "Smart wall model for molecular dynamics simulations of nanoscale gas flows," Commun. Comput. Phys. **7**, 977–993 (2010).
[36] M. Barisik and A. Beskok, "MD simulations of nano-scale gas flows: A case study of Couette flow at Kn = 10," AIP Conf. Proc. **1333**, 707–711 (2011).
[37] M. Barisik and A. Beskok, "Surface-gas interaction effects on nanoscale gas flows," Microfluidics Nanofluidics **13**(5), 789–798 (2012).
[38] M. Barisik and A. Beskok, "Molecular dynamics simulations of shear driven gas flows in nano-channels," Microfluidics Nanofluidics **11**(5), 611–622 (2011).
[39] M. Barisik and A. Beskok, "Equilibrium molecular dynamics studies on nanoscale-confined fluids," Microfluidics Nanofluidics **11**(3), 269–282 (2011).
[40] J. C. Maxwell, "On stresses in rarified gases arising from inequalities of temperature," Philos. Trans. R. Soc. London **170**, 231 (1879).
[41] C. Cercignani and M. Lampis, "Kinetic models for gas-surface interactions," Transp. Theory Stat. Phys. **1**, 101–114 (1971).
[42] A. Beskok and G. E. Karniadakis, "A model for flows in channels, pipes and ducts at micro and nano scales," Microscale Thermophys. Eng. **3**(1), 43–77 (1999).
[43] F. J. Alexander and A. L. Garcia, "The direct simulation Monte Carlo method," Comput. Phys. **11**(6), 588 (1997).
[44] M. P. Allen and D. J. Tildesley, *Computer Simulation of Liquids* (Oxford Science Publications, New York, 1989).
[45] D. J. Evans and W. G. Hoover, "Flows far from equilibrium via molecular-dynamics," Annu. Rev. Fluid Mech. **18**, 243–264 (1986).
[46] T. Ohwada, Y. Sone, and K. Aoki, "Numerical analysis of the Poiseuille and thermal transpiration flows between two parallel plates on the basis of the Boltzmann equation for hard-sphere molecules," Phys. Fluids A **1**, 2042 (1989).
[47] F. Sharipov, "Application of the Cercignani-Lampis scattering kernel to channel gas flows," AIP Conf. Proc. **585**, 347 (2001).
[48] M. Knudsen, "Die Gesetze der Molekularstromung und der innern Reibungsstromung der Gase durch Rohren," Ann. Phys. **333**, 75–130 (1909).
[49] W. Gaede, "Die äussere Reibung der Gase," Ann. Phys. **346**, 289 (1913).
[50] S. A. Tison, "Experimental data and theoretical modeling of gas flows through metal capillary leaks," Vacuum **44**(11), 1171–1175 (1993).
[51] C. Cercignani and A. Daneri, "Flow of a rarefied gas between two parallel plates," J. Appl. Phys. **34**(12), 3509–3513 (1963).
[52] S. K. Loyalka and S. A. Hamoodi, "Poiseuille flow of a rarefied gas in a cylindrical tube: Solution of linearized Boltzmann equation," Phys. Fluids A **2**, 2061–2065 (1990).
[53] W. G. Pollard and R. D. Present, "On gaseous self-diffusion in long capillary tubes," Phys. Rev. **73**(7), 762–774 (1948).